



Metal-organic framework/carbon nanotube-coated polyethylene separator for improving the cycling performance of lithium-sulfur cells

Dae Hee Lee ^{a,b}, Jun Hwan Ahn ^a, Myung-Soo Park ^a, Ali Eftekhari ^c, Dong-Won Kim ^{a,*}

^a Department of Chemical Engineering, Hanyang University, Seoul 04763, South Korea

^b Cell Development Group, Samsung SDI, Chungcheongnam-do 31086, South Korea

^c Belfast Academy, 2 Queens Road, Belfast BT3 9FG, United Kingdom



ARTICLE INFO

Article history:

Received 5 April 2018

Received in revised form

7 July 2018

Accepted 8 July 2018

Keywords:

Lithium-sulfur cell

Metal organic framework

Multi-wall carbon nanotube

Lithium polysulfide

Functionalized separator

ABSTRACT

Since the so-called 'shuttle effect' is the key obstacle for the practical development of lithium-sulfur batteries, the present attempt is to make the separator less permeable for polysulfides. For this purpose, we synthesized Ni-based metal-organic framework (Ni-MOF) particles and coated them with multi-walled carbon nanotubes (MWCNTs) onto the polyethylene (PE) separator. The Ni-MOF particles on separator effectively blocked the migration of lithium polysulfides toward the anode side owing to the strong interaction between Ni-MOFs and lithium polysulfides. The highly conductive MWCNTs in the coating layer allowed reutilization of the trapped reaction intermediates during the subsequent cycles. Due to these beneficial effects of coating materials, the lithium-sulfur cell assembled with Ni-MOF/MWCNT-coated PE separator initially delivered a high discharge capacity of 1358 mAh g⁻¹ with good cycling stability and high-rate performance.

© 2018 Elsevier Ltd. All rights reserved.

1. Introduction

Rechargeable lithium batteries as the prime choices in a variety of applications, such as mobile electronic devices, electric vehicles and large-scale energy storage systems, have been actively studied over several decades [1–3]. Among the emerging types of lithium batteries, lithium-sulfur battery has been attracted considerable attention due to its high energy density, low price and environmental friendliness [4–8]. However, several critical problems, such as the low utilization of sulfur, poor cycle life and low rate capability have hindered its practical applications. These hurdles are mainly ascribed to the low conductivity of sulfur and polysulfide intermediates, and shuttle effect arising from the lithium polysulfides dissolved in the electrolyte solution, which result in the gradual loss of the active materials, the rapid decline of reversible capacity and poor rate capability [9–11]. To solve these problems, sulfur was confined in porous and conductive framework materials, such as conductive porous carbons [8,12–16], carbon nanotubes [17–20], electronically conductive polymers [21–23],

graphene-derived materials [24–27], metal oxides [28–30], magnetic nanoparticles [31,32] and metal-organic framework (MOF)-based materials [33–38]. These approaches improved the cycling performance of lithium-sulfur batteries to some extent. However, the electrode fabrication processes are cumbersome and time-consuming, particularly at large scale, and the lithium polysulfide migration from the sulfur cathode to the lithium anode side still occurs. Recently, utilizing the modified functional separators with various porous and conductive materials has drawn attention for restraining the lithium polysulfide migration [39–43]. Among the functional materials for modifying the conventional separators, MOF is regarded as a promising candidate because of its high porosity and large surface area. In addition, open metal sites of MOF can interact with lithium polysulfides to hinder the transport of lithium polysulfides toward the anode side. Although MOF has been exploited as a sulfur host in lithium-sulfur batteries owing to the ability to confine polysulfides [33–38,44,45], its electronic conductivity is so low that a significant amount of conductive additive is required to achieve acceptable electrochemical performance. The weight of these additives obviously reduces the energy density of the cell. Therefore, it is more advantageous to use MOF as a coating material for modifying the separator used in the lithium-sulfur cell.

* Corresponding author.

E-mail address: dongwonkim@hanyang.ac.kr (D.-W. Kim).

In this work, we synthesized nano-sized Ni-MOF-74 (Ni-MOF) with high surface area and pore volume. Ni-MOF has one-dimensional pores which serve as the diffusion channels for the Li-ions. Moreover, Ni²⁺ sites in Ni-MOF exhibit Lewis acidic characteristics, which induce strong interaction with polysulfide anions due to their soft Lewis basic property by lone electron pairs in sulfur [33,46,47]. The obtained Ni-MOF particles were coated onto a polyethylene (PE) separator with multi-walled carbon nanotubes (MWCNTs) by a simple vacuum-filtration method. MWNT was used to enhance the electronic conductivity and prevent the migration of polysulfides as a physical barrier. The lithium-sulfur cell assembled with Ni-MOF/MWCNT-coated PE separator exhibited a high initial discharge capacity of 1358 mAh g⁻¹ with good capacity retention and enhanced rate capability. Such a superior cycling performance is attributed to not only the effective suppression of the migration of polysulfides to the anode side due to the strong interaction between open nickel²⁺ sites of Ni-MOF and polysulfides but also the enhanced sulfur utilization.

2. Experimental

2.1. Synthesis of nanoscaled Ni-MOF

Nanosized Ni-MOF was synthesized according to previous reports [48,49]. In a typical synthesis procedure, 0.2 g of 2,5-dihydroxyterephthalic acid was dissolved in 5.0 g of *N,N*-dimethylformamide (DMF) under stirring for 10 min to form a homogeneous yellow solution. Then, 0.65 g of nickel acetate tetrahydrate dissolved in DMF was added to the solution resulting in an immediate formation of blue-green precipitates. The mixture was kept at room temperature for 20 h. The solid product was collected by centrifuge and washed with DMF and methanol several times. Finally, the obtained Ni-MOF was vacuum dried at 40 °C for 12 h.

2.2. Coating of Ni-MOF and MWCNT onto PE separator

Both Ni-MOF and MWCNT were coated onto PE separator by vacuum-filtration method. To prepare the coating solution, an equal amount (2.0 mg) of Ni-MOF and MWCNT was added to 500 mL of ethanol, and the mixture was homogeneously dispersed using sonication for 3 h. The obtained solution was vacuum filtered through a PE separator (Asahi ND420, thickness: 20 μm) to coat the mixture of Ni-MOF and MWCNT onto one side of the PE separator. The Ni-MOF/MWCNT-coated separator was dried in a vacuum oven at 60 °C for 12 h. The total mass of the coating materials (Ni-MOF and MWCNT) on the PE separator was about 0.36 mg cm⁻² and the final mass of Ni-MOF/MWCNT-coated separator was about 1.58 mg cm⁻², corresponding to 29.5% increase in weight as compared to pristine PE separator. An MWCNT-coated separator was also prepared as a reference sample with the same procedure.

2.3. Assembly of lithium-sulfur cells

The sulfur cathode was prepared by coating *N*-methyl pyrrolidinone (NMP)-based slurry containing 60 wt% sulfur powder (Sigma-Aldrich), 30 wt% Super-P carbon (MMM co.) and 10 wt% poly(vinylidene fluoride) (PVDF, Solvay) onto an aluminum foil. The mass loading of active sulfur in the cathode was about 2.0 mg cm⁻². The anode was prepared by pressing 200 μm-thick lithium foil (Honjo Metal Co. Ltd.) onto a copper current collector. The lithium-sulfur cell was assembled by sandwiching Ni-MOF/MWCNT-coated separator between the lithium anode and the sulfur cathode in a

CR2032-type coin cell. The cell was then injected with liquid electrolyte consisting of 1.0 M lithium bis(trifluoromethanesulfonyl)imide ($\text{LiN}(\text{SO}_2\text{CF}_3)_2$, LiTFSI) dissolved in a mixed solvent of 1,3-dioxolane (DOL) and 1,2-dimethoxyethane (DME) (50:50 by volume) containing 0.4 M LiNO₃ (battery grade, PANAX ETEC Co. Ltd.). LiNO₃ was added to liquid electrolyte as an additive to obtain good cycling performance in all the cells investigated. The amount of liquid electrolyte was controlled to be 60 μL per 1.0 mg of sulfur in the cathode. All cells were assembled in a dry box filled with argon gas.

2.4. Characterizations and measurements

The crystalline phase of Ni-MOF was examined by X-ray diffraction (XRD) (miniFlex600, Rigaku) using Cu K ($\lambda = 0.15 \text{ nm}$) radiation. The morphologies of Ni-MOF and Ni-MOF/MWCNT-coated PE separator were investigated using scanning electron microscope (JEOL JSM 6701F) and transmission electron microscope (JEOL 2100F). Surface elemental characterization of the Ni-MOF/MWCNT-coated PE separator was conducted using energy dispersive spectrometer (EDS). To measure Brunauer-Emmett-Teller (BET) surface area and pore size distribution of Ni-MOF, nitrogen adsorption/desorption isotherms were obtained at -196 °C using Micromeritics 3 Flex. In order to investigate the interaction between of Ni-MOF with Li₂S₄, 4 mg of Li₂S₄ was dissolved in 5 mL of tetrahydrofuran (THF) and 20 mg of Ni-MOF was added into the solution. The solution was further stirred for 1 h and the precipitated product was collected after 12 h. The product was then completely dried under vacuum at 60 °C for 12 h to remove residual THF, and X-ray photoelectron spectroscopy (XPS, VG ESCALAB 220i) analysis was carried out. Electrochemical impedance spectroscopy was performed using a Zahner Electrik IM6 impedance analyzer. The frequency range was from 100 kHz to 0.1 Hz with AC voltage amplitude of 10 mV. Charge and discharge cycling tests of the cells were carried out at a current rate of 0.2 C and 25 °C over a voltage range of 1.8–2.6 V using battery testing equipment (WBCS 3000, WonA Tech Co., Ltd.).

3. Results and discussion

Ni-MOF is a one-dimensional porous crystalline material that has open nickel²⁺ sites and organic aromatic linkers, as shown in Fig. 1(a). The crystalline peaks observed in XRD pattern of Ni-MOF powder (Fig. 1(b)) correspond to the Miller index (110) and (300). The peaks have broad shapes, indicating that the synthesized Ni-MOF material has small crystal size [48]. Fig. 1(c) and (d) show the TEM images of nano-sized Ni-MOF material with two different magnifications, which illustrate that Ni-MOFs are nano-sized particles with uniform porous structure. EDS mapping images of Ni-MOF sample are depicted Fig. 2, showing the presence and uniform distribution of nickel, oxygen and carbon elements in Ni-MOF.

To measure the surface area and pore size distribution of Ni-MOF sample, N₂ adsorption/desorption isotherms were obtained, as given in Fig. 3(a). It exhibits type I isotherms curve according to the IUPAC classification with a sharp adsorption shape at a relative pressure below 0.1 [50], indicating that the pores in Ni-MOF are mainly micropores. This result is consistent with pore size distribution of Ni-MOF in Fig. 3(b), which shows the existence of many micropores below pore size of 2 nm. The total and micropore volumes in Ni-MOF sample were measured to be 0.35 and 0.30 cm³ g⁻¹, respectively. BET surface area of Ni-MOF was determined to be 868 m² g⁻¹ with a microporous surface area of 793 m² g⁻¹. Note that the BET surface area of MWCNT was about 177 m² g⁻¹. Large surface area of Ni-MOF can provide an

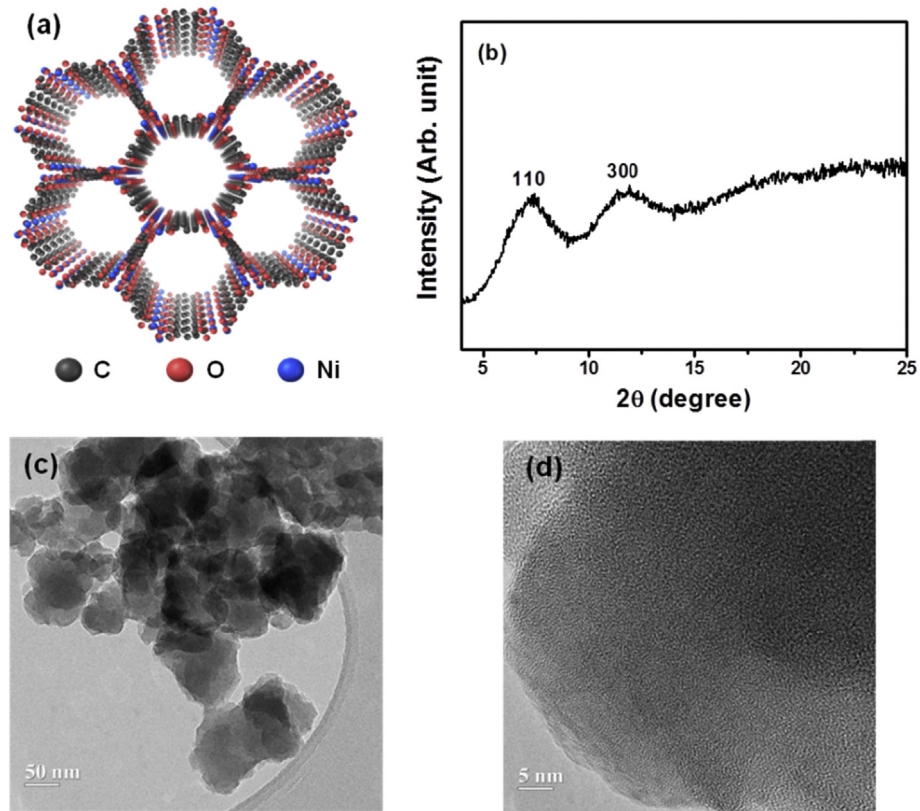


Fig. 1. (a) Crystalline structure and (b) XRD pattern of Ni-MOF material. TEM images of nano-sized Ni-MOF particles with (c) lower and (d) higher magnifications.

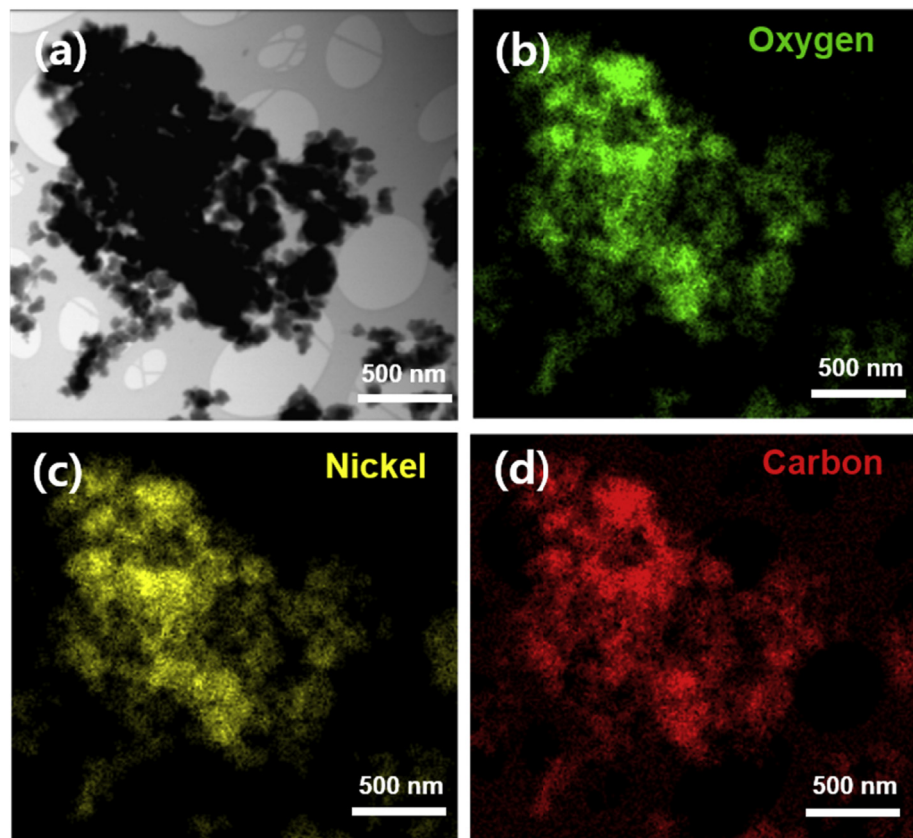


Fig. 2. (a) TEM image and EDS mapping images of (b) O, (c) Ni and (d) C of the Ni-MOF particles.

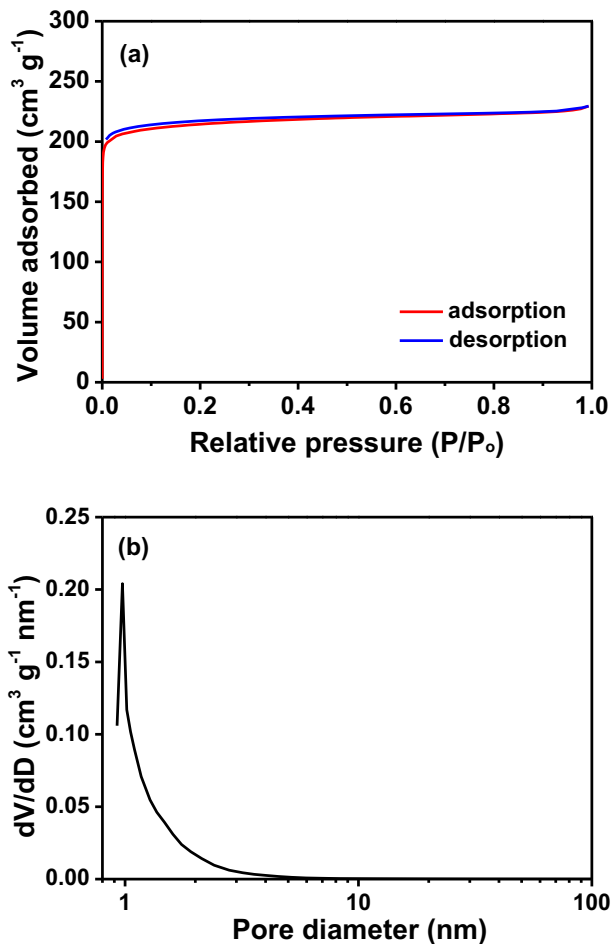


Fig. 3. (a) N_2 adsorption/desorption isotherms and (b) pore size distribution of Ni-MOF.

opportunity for the interaction between lithium polysulfides and open metal sites of Ni-MOF. Raman spectrum of MWCNT is shown in Fig. S1(a). The obtained peaks at 1571 and 1342 cm^{-1} correspond to G band of sp^2 hybridized graphitic structure and D band of sp^3 disordered carbon, respectively [51]. The intensity ratio of the D to G band (I_D/I_G) was calculated to be 0.708, indicating relatively less defects in MWCNT. Fig. S1(b) presents the XRD patterns of MWCNT and Ni-MOF/MWCNT composite. The crystalline peaks at 25.9° and 44.7° in 2θ are attributed to the (002) and (100) planes of MWCNT, respectively [52]. In the Ni-MOF/MWCNT composite, the crystalline peaks of Ni-MOF could be also observed in the 2θ range of 7 to 14° .

Ni-MOF and MWCNT were coated onto one side of a PE separator. Fig. 4 is a schematic illustration showing the prohibiting role of the Ni-MOF/MWCNT-coated PE separator against the shuttle effect in the lithium-sulfur cell. The coating layer consisting of Ni-MOF and MWCNT faced to the sulfur cathode is expected to effectively block the migration of lithium polysulfides during the repeated cycling in the lithium-sulfur cell. During the discharge cycle, the soluble lithium polysulfides can be immobilized by interaction between the coordinately unsaturated sites of Ni-MOF and lithium polysulfides. In the coating layer, MWCNTs not only act as a physical barrier that retards the diffusion of lithium polysulfides toward anode side but also enhance the electronic conductivity of trapped lithium polysulfides for the subsequent electrochemical reaction [53–55]. On the other hand, Ni-MOF can effectively trap lithium polysulfides by Lewis acid-base interaction. As previously reported [33,46,47], the Ni^{2+} sites in Ni-MOF exhibit Lewis acidic characteristics, which promotes strong interaction with polysulfide anions due to their soft Lewis basic character induced by lone-paired electron in sulfur. Low electronic conductivity of Ni-MOF can be compensated by adding highly conductive MWCNTs into the coating layer, facilitating charge transfer reaction of trapped lithium polysulfides for subsequent cycling.

Fig. 5 shows the SEM and EDS elemental mapping images of the

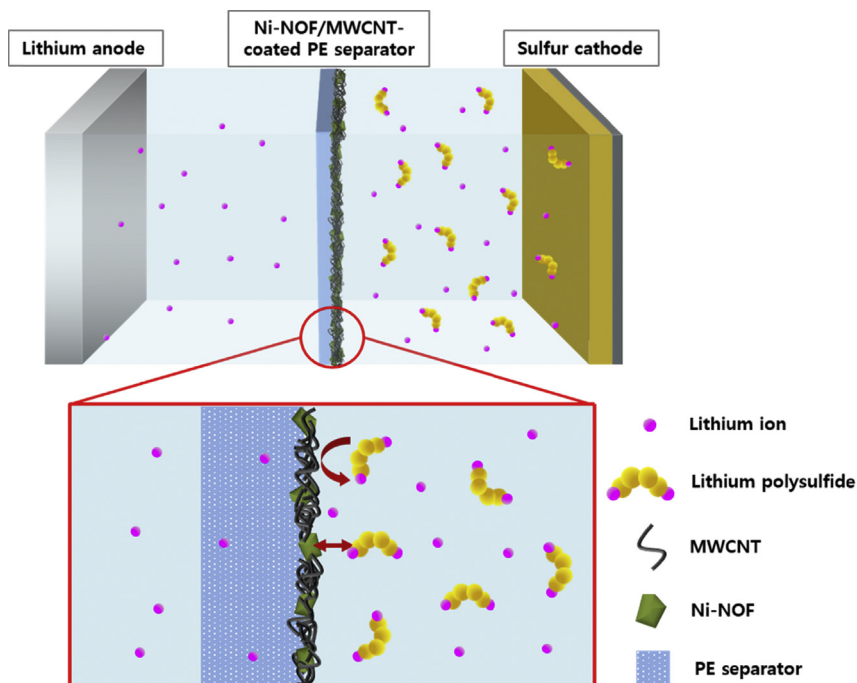


Fig. 4. Schematic illustration of Ni-MOF/MWCNT-coated PE separator for blocking lithium polysulfide migration to the lithium anode in the lithium-sulfur cell.

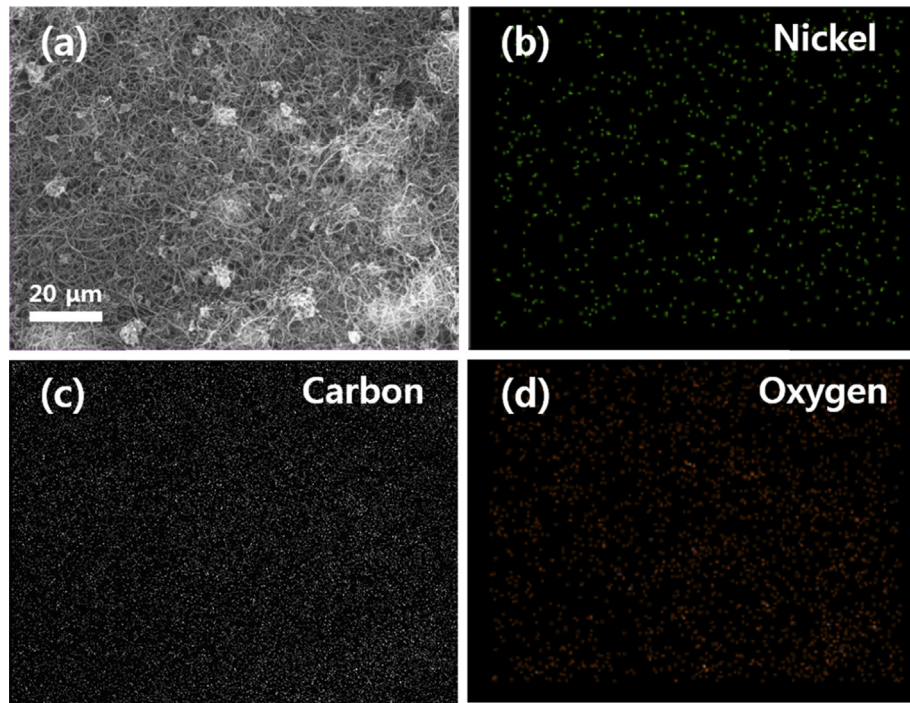


Fig. 5. (a) SEM image of Ni-MOF/MWCNT-coated separator and EDS mapping images of (b) Ni, (c) C and (d) O on the Ni-MOF/MWCNT-coated separator.

surface of Ni-MOF/MWCNT-coated PE separator. After immobilizing Ni-MOF and MWCNT onto the PE separator, the separator still maintained the porous structure allowing the transport of lithium ions through the separator. As shown in Fig. 5(b)–(d), the Ni-MOF/MWCNT-coated PE separator shows a uniform distribution of nickel, carbon and oxygen elements in the SEM-EDS elemental mapping of the surface, which confirms that the PE separator is

uniformly coated with Ni-MOF and MWCNT. These results demonstrate that the vacuum filtration is a favorable method to uniformly spread the nano-sized Ni-MOF particles and MWCNTs onto the PE separator. The total mass of Ni-MOF and MWCNT coated on the PE separator was about 0.36 mg cm^{-2} . The cross-sectional SEM image of the Ni-MOF/MWCNT-coated PE separator is presented in Fig. S2. Upper part on PE separator corresponds to the

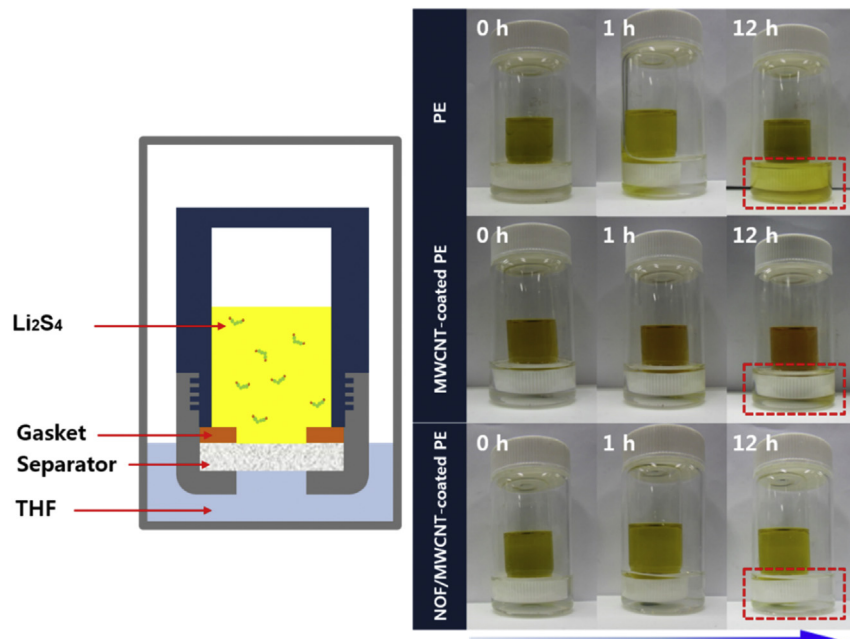


Fig. 6. Schematic illustration showing migration test of Li_2S_4 (left). In the photographs of right vial solutions, the migration of Li_2S_4 through different separators was monitored.

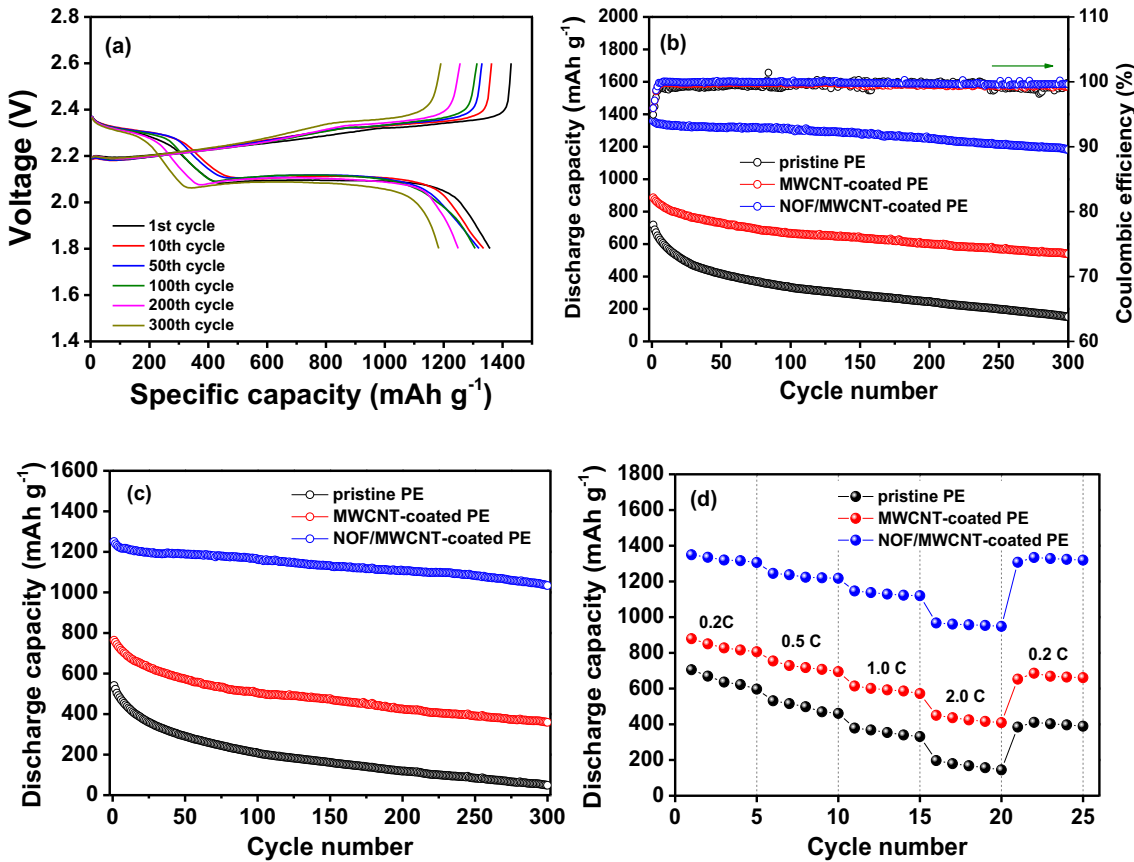


Fig. 7. (a) Charge and discharge curves of the lithium sulfur-cell with Ni-MOF/MWCNT-coated separator at 0.2 C rate. Cycling performance of the lithium-sulfur cells assembled with different separators at (b) 0.2 C rate and (c) 0.5 C rate. (d) Rate capability of the lithium-sulfur cells with the C rate increasing from 0.2 to 2.0 C every five cycles.

coating layer composed of Ni-MOF and MWCNT, and the thickness of the Ni-MOF/MWCNT coating layer is measured to be 8.25 μm based on the image.

To investigate the migration behavior of lithium polysulfides through the Ni-MOF/MWCNT-coated PE separator, the migration test of Li_2S_4 was carried out, as illustrated in the left side of Fig. 6. In this test, a vial containing a solution of Li_2S_4 (8 mg) dissolved in a mixed solvent of DME and DOL (10 ml) was prepared. The solution in vial was allowed to migrate through the separator to another vial containing a solvent mixture without the dissolved polysulfide, and the color change was monitored with time [43]. In the case of the pristine PE separator, the color of the solvent turned from colorless to yellow, indicating the migration of dissolved lithium polysulfide through the PE separator. When using the MWCNT-coated separator, the color of the solvent remained intact after 1 h. However, it became light yellow after 12 h due to the diffusion of a small amount of lithium polysulfides. In contrast, there was no color change in a vial with Ni-MOF/MWCNT-coated separator, indicating that most of the lithium polysulfides were trapped by the coating layer composed of Ni-MOF and MWCNT due to the strong interaction between Ni-MOF and lithium polysulfides.

Cycling performance of the lithium-sulfur cells with different separators was evaluated at 0.2 C rate, and the charge-discharge curves of the cell using Ni-MOF/MWCNT-coated separator are shown in Fig. 7(a). The voltage profiles exhibit two discharge plateaus and a long charge plateau. The discharge plateaus at about 2.3 and 2.0 V can be ascribed to the reduction of elemental

sulfur (S_8) to the long-chain polysulfide (Li_2S_n , $4 \leq n \leq 8$), and the reduction of long-chain polysulfide to insoluble lithium sulfides ($\text{Li}_2\text{S}_2/\text{Li}_2\text{S}$), respectively. The long charge plateau corresponds to the oxidation of Li_2S_2 and Li_2S to cyclic sulfur. The voltage profiles of the cell employing the Ni-MOF/MWCNT-coated separator are very stable with cycling, and the cell shows low overpotential during cycling. For comparison, the charge and discharge curves of the lithium-sulfur cells assembled with pristine PE separator and MWCNT-coated separator are also shown in Fig. S3. All cells exhibit the similar voltage profiles showing two discharge plateaus and a long charge plateau. It should be noted that the specific capacities corresponding to the lower discharge plateau in these cells are small when comparing to the cell with Ni-MOF/MWCNT-coated separator, and the capacity during the lower discharge plateau is least for the cell with the pristine PE separator. These results imply that the formed soluble lithium polysulfides are not effectively utilized during subsequent reactions in the cell with the pristine separator due to the migration of soluble polysulfides to the anode side, thereby resulting in reduced capacity during the lower discharge plateau. Cycling performance of the lithium-sulfur cells with different types of separators is compared in Fig. 7(b). The cell with pristine PE separator suffered from large capacity fading during cycling, which results from the continuous loss of active sulfur due to the dissolution of lithium polysulfides into the electrolyte solution and their migration to the anode side, as mentioned earlier. Although the cell with MWCNT-coated separator exhibited better capacity retention as compared to the cell using pristine PE separator, its cycling stability was

inferior to the cell employing the Ni-MOF/MWCNT-coated separator. In contrast, the cell with Ni-MOF/MWCNT-coated separator delivered a high discharge capacity of 1183 mAh g^{-1} after 300 cycles, which corresponded to 87.1% of its initial capacity. When comparing Coulombic efficiencies of three cells, the cell with Ni-MOF/MWCNT-coated separator showed the highest and the most stable values during the repeated cycling among the cells. As explained in Fig. 6, most of the lithium polysulfides are trapped in the coating layer composed of Ni-MOF and MWCNT, and they can be reutilized in the subsequent cycles, which results in the stabilization and improvement of Coulombic efficiency. Cycling performance of the lithium-sulfur cells at higher current rate (0.5 C) is also compared in Fig. 7(c). Clearly, the cell with Ni-MOF/MWCNT-coated separator showed the best cycling characteristics in terms of discharge capacity and capacity retention. Fig. 7(d) presents the discharge capacities of the lithium-sulfur cells with different separators, during experiments in which the C rate was increased from 0.2 to 2.0 C every five cycles. As expected, the discharge capacities gradually decreased with increasing C rate due to the polarization. Among the cells, the cell with Ni-MOF/MWCNT-coated separator exhibited the highest discharge capacities at all C rates investigated. The cell with Ni-MOF/MWCNT-coated separator delivered a high discharge capacity of 968 mAh g^{-1} at 2.0 C, while the cells with PE separator and MWCNT-coated separator exhibited lower discharge capacities of 197 and 451 mAh g^{-1} , respectively. The enhanced high rate performance can be mostly attributed to the improved electronic conductivity due to the presence of conductive MWCNT and suppression of polysulfide migration due to its effective trap in Ni-MOF.

We obtained the AC impedance spectra of the cells with three different types of separator after the 1st and 300th cycles, and the results are given in Fig. 8. All the cells exhibited two overlapping semicircles due to different combinations of interfacial resistances and capacitances, with the real axis intercept corresponding to the electrolyte resistance (R_e). The first semicircle observed in the higher frequency range arises from resistance due to Li^+ ion migration through the surface film on the electrode (R_f), and the second semicircle in the middle to low-frequency range was attributed to charge transfer reaction at the electrode-electrolyte interface (R_{ct}). After the first cycle, the cells showed almost same resistances. However, the cells gave quite different results after 300 cycles. In the cell with pristine PE separator, both electrolyte resistance and interfacial resistance remarkably increased after 300 cycles. A large increase in the electrolyte resistance in this cell is mainly attributed to the increase in viscosity of electrolyte solution due to the dissolution of lithium polysulfides into the solution during cycling. At the same time, the interfacial resistances were also rapidly increased due to the retardation of the charge transfer reaction at the electrolyte-electrode interface. Interestingly, the cell with Ni-MOF/MWCNT-coated separator showed little increase in electrolyte resistance and interfacial resistances even after the repeated cycling, resulted in the lowest resistances among the cells. These results demonstrate that the combination of Ni-MOF and MWCNT effectively trapped and reutilized soluble lithium polysulfides within the cathode side resulting in reduced R_e , R_f and R_{ct} during cycling. Due to the suppression of lithium polysulfide migration and the enhanced reutilization of lithium polysulfide trapped in the coating layer, the cell with Ni-MOF/MWCNT-coated separator exhibited a superior cycling performance than other two cells.

The interaction between of Ni-MOF with Li_2S_4 was investigated by S 2p and Ni 2p XPS spectra shown in Fig. 9. In the S 2p XPS spectrum of Li_2S_4 , two peaks are observed at 161.1 and 162.8 eV, which correspond to the terminal sulfur (S_{T}^{2-}) and bridging sulfur (S_{B}^0) atoms, respectively [29,56]. In the Ni 2p XPS spectra of Ni-MOF,

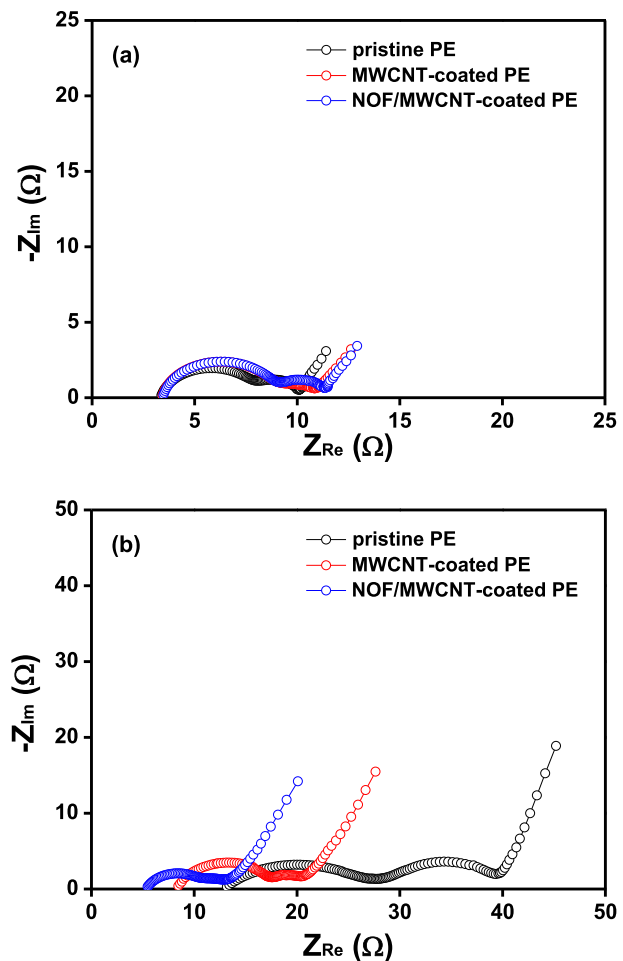


Fig. 8. AC impedance spectra of the lithium-sulfur cells assembled with different separators, which were obtained (a) after the 1st and (b) 300th cycles.

there are two peaks at 855.7 and 874.0 eV, which can be assigned to Ni 2p_{1/2} and Ni 2p_{3/2}, respectively [57]. In the Li_2S_4 -Ni-MOF mixture, the S 2p peaks were shifted to 161.8 and 163.8 eV, while the Ni 2p peaks were shifted to 854.8 and 873.1 eV. The S 2p peak observed at 168 eV corresponds to the binding energy of sulfate species, which arises from the oxidation between Li_2S_4 and oxygen of Ni-MOF. Since the Ni-based coordinatively unsaturated sites of Ni-MOF react with fluid molecules such as lithium polysulfides [33,34], they could form a coordinate bond with Li_2S_4 . As a result, the chemical interaction between Ni and negatively charged Li_2S_4 lowered the binding energy of Ni [58]. From these results, a strong interaction between lithium polysulfides and Ni in Ni-MOF could be confirmed.

4. Conclusions

A functional separator was prepared by coating Ni-MOF and MWCNT onto PE separator using simple vacuum filtration method. The Ni-MOF/MWCNT-coated PE separator effectively suppressed the migration of lithium polysulfides toward anode side by trapping polysulfides in the coating layer. The presence of MWCNT in the coating layer not only enhanced the electronic conductivity for reutilization of lithium polysulfides but also played a role as a physical barrier blocking the diffusion of lithium polysulfide. As a result, the lithium-sulfur cell with Ni-MOF/

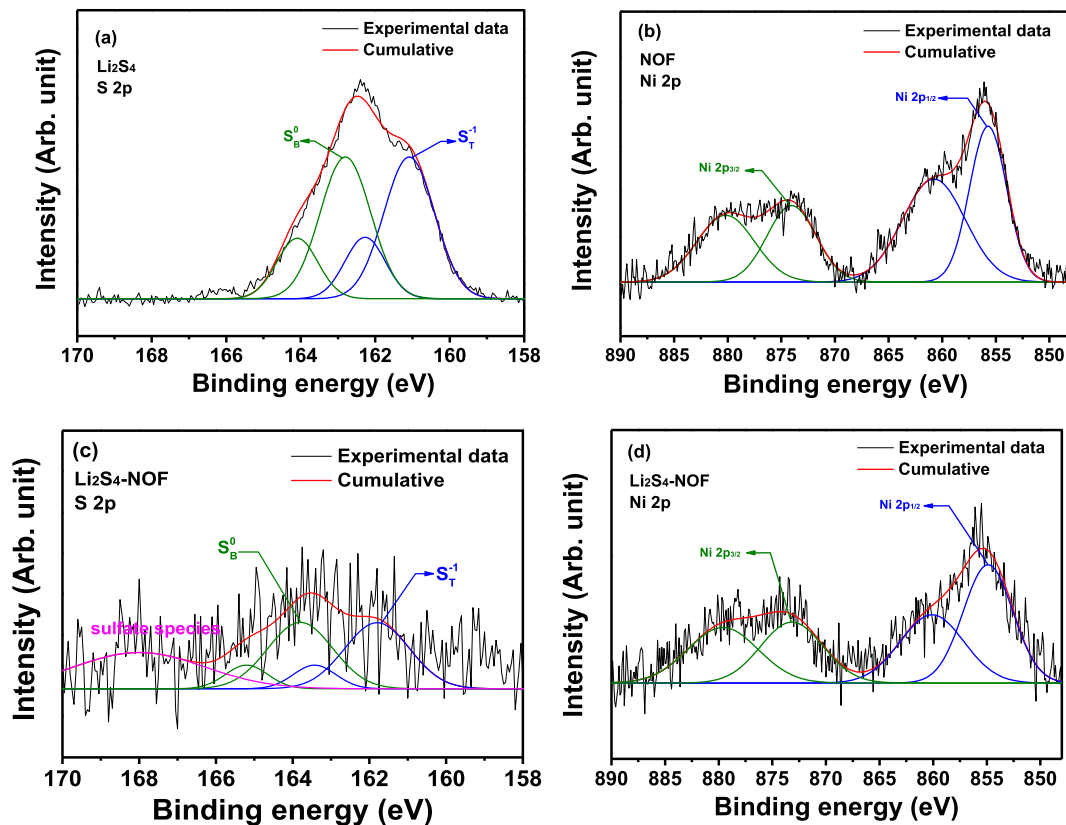


Fig. 9. (a) XPS S 2p spectrum of Li_2S_4 and (b) Ni 2p spectrum of Ni-MOF. (c) XPS S 2p and (d) Ni 2p spectra of Li_2S_4 -Ni-MOF mixture.

MWCNT-coated PE separator delivered a high discharge capacity of 1358 mAh g⁻¹ with good capacity retention and exhibited an improved rate capability. Consequently, the separator coated with Ni-MOF and MWCNT in this study can be a promising one for the high energy-density lithium-sulfur batteries with good cycling stability.

Acknowledgements

This work was supported by the Basic Science Research Program of the National Research Foundation of Korea (NRF), funded by the Ministry of Science, ICT, and Future Planning (2017R1A2A2A05020947).

Appendix A. Supplementary data

Supplementary data related to this article can be found at <https://doi.org/10.1016/j.electacta.2018.07.031>.

References

- [1] M. Armand, J.M. Tarascon, Building better batteries, *Nature* 451 (2008) 652–657.
- [2] C. Liu, F. Li, L.P. Ma, H.M. Cheng, Advanced materials for energy storage, *Adv. Mater.* 22 (2010) E28–E62.
- [3] B. Dunn, H. Kamath, J.M. Tarascon, Electrical energy storage for the grid: a battery of choices, *Science* 334 (2011) 928–935.
- [4] X.L. Ji, L.F. Nazar, Advances in Li-S batteries, *J. Mater. Chem.* 20 (2010) 9821–9826.
- [5] J. Kim, D.J. Lee, H.G. Jung, Y.K. Sun, J. Hassoun, B. Scrosati, An advanced lithium-sulfur battery, *Adv. Funct. Mater.* 23 (2013) 1076–1080.
- [6] A. Manthiram, Y. Fu, S.H. Chung, C. Zu, Y.S. Su, Rechargeable lithium-sulfur batteries, *Chem. Rev.* 114 (2014) 11751–11787.
- [7] A. Manthiram, S.H. Chung, C. Zu, Lithium-sulfur batteries: progress and prospects, *Adv. Mater.* 27 (2015) 1980–2006.
- [8] A. Eftekhar, D.-W. Kim, Cathode materials for lithium-sulfur batteries: a practical perspective, *J. Mater. Chem. A* 5 (2017) 17734–17776.
- [9] Y.V. Mikhaylik, J.R. Akridge, Polysulfide shuttle study in the Li/S battery system, *J. Electrochem. Soc.* 151 (2004) A1969–A1976.
- [10] R. Xu, I. Belharouak, X. Zhang, R. Chamoun, C. Yu, Y. Ren, A. Nie, R. Shahbazian-Yassar, J. Lu, J.C. Li, K. Amine, Insight into sulfur reactions in Li-S batteries, *ACS Appl. Mater. Interfaces* 6 (2014) 21938–21945.
- [11] Y. Diao, K. Xie, S.Z. Xiong, X.B. Hong, Shuttle phenomenon – the irreversible oxidation mechanism of sulfur active material in Li-S battery, *J. Power Sources* 235 (2013) 181–186.
- [12] X. Ji, K.T. Lee, L.F. Nazar, A highly ordered nanostructured carbon-sulfur cathode for lithium-sulfur batteries, *Nat. Mater.* 8 (2009) 500–506.
- [13] H. Ye, Y.X. Yin, S. Xin, Y.G. Guo, Tuning the porous structure of carbon hosts for loading sulfur toward long lifespan cathode materials for Li-S batteries, *J. Mater. Chem. A* 1 (2013) 6602–6608.
- [14] J. Schuster, G. He, B. Mandlmeier, T. Yim, K.T. Lee, T. Bein, L.F. Nazar, Spherical ordered mesoporous carbon nanoparticles with high porosity for lithium-sulfur batteries, *Angew. Chem. Int. Ed.* 51 (2012) 3591–3595.
- [15] C. Lai, X.P. Gao, B. Zhang, T.Y. Yan, Z. Zhou, Synthesis and electrochemical performance of sulfur/highly porous carbon composites, *J. Phys. Chem. C* 113 (2009) 4712–4716.
- [16] Z. Gao, Y. Zhang, N. Song, X. Li, Towards flexible lithium-sulfur battery from natural cotton textile, *Electrochim. Acta* 246 (2017) 507–516.
- [17] S. Xin, L. Gu, N.H. Zhao, Y.X. Yin, L.J. Zhou, Y.G. Guo, L.J. Wan, Smaller sulfur molecules promise better lithium-sulfur batteries, *J. Am. Chem. Soc.* 134 (2012) 18510–18513.
- [18] F. Wu, J. Qian, R.J. Chen, T. Zhao, R. Xu, Y.S. Ye, W.H. Li, L. Li, J. Lu, K. Amine, Sulfur cathode based on layered carbon matrix for high-performance Li-S batteries, *Nano Energy* 12 (2015) 742–749.
- [19] J.Z. Chen, D.X. Wu, E. Walter, M. Engelhard, P. Bhattacharya, H.L. Pan, Y.Y. Shao, F. Gao, J. Xiao, J. Liu, Molecular-confinement of polysulfides within mesoscale electrodes for the practical application of lithium sulfur batteries, *Nano Energy* 13 (2015) 267–274.
- [20] C. Xu, H. Zhou, C. Fu, Y. Huang, L. Chen, L. Yang, Y. Kuang, Hydrothermal synthesis of boron-doped unzipped carbon nanotubes/sulfur composite for high-performance lithium-sulfur batteries, *Electrochim. Acta* 232 (2017) 156–163.
- [21] J. Wang, K. Yue, X. Zhu, K.L. Wang, L. Duan, C-S@PANI composite with a polymer spherical network structure for high performance lithium-sulfur batteries, *Phys. Chem. Chem. Phys.* 18 (2016) 261–266.
- [22] L. Xiao, Y. Cao, J. Xiao, B. Schwenzler, M.H. Engelhard, L.V. Saraf, Z. Nie,

- G.J. Exarhos, J. Liu, A soft approach to encapsulate sulfur: polyaniline nanotubes for lithium-sulfur batteries with long cycle life, *Adv. Mater.* 24 (2012) 1176–1181.
- [23] Y. Liu, W. Yan, X. An, X. Du, Z. Wang, H. Fan, S. Liu, X. Hao, G. Guan, A polypyrrole hollow nanosphere with ultra-thin wrinkled shell: synergistic trapping of sulfur in Lithium–sulfur batteries with excellent elasticity and buffer capability, *Electrochim. Acta* 271 (2018) 67–76.
- [24] G.M. Zhou, L. Li, C.Q. Ma, S.G. Wang, Y. Shi, N. Koratkar, W.C. Ren, F. Li, H.M. Cheng, A graphene foam electrode with high sulfur loading for flexible and high energy Li–S batteries, *Nano Energy* 11 (2015) 356–365.
- [25] Y. You, W.C. Zeng, Y.X. Yin, J. Zhang, C.P. Yang, Y.W. Zhu, Y.G. Guo, Hierarchically micro/mesoporous activated graphene with a large surface area for high sulfur loading in Li–S batteries, *J. Mater. Chem. A* 3 (2015) 4799–4802.
- [26] W.C. Du, J. Zhang, Y.X. Yin, Y.G. Guo, L.J. Wan, Sulfur confined in sub-nanometer-sized 2D graphene interlayers and its electrochemical behavior in lithium–sulfur batteries, *Chem. Asian J.* 11 (2016) 2690–2694.
- [27] Z. Wu, W. Wang, Y.T. Wang, C. Chen, K.L. Li, G.J. Zhao, C.Y. Sun, W.J. Chen, L.B. Ni, G.W. Diao, Three-dimensional graphene hollow spheres with high sulfur loading for high-performance lithium-sulfur batteries, *Electrochim. Acta* 224 (2017) 527–533.
- [28] Z. Wei Seh, W. Li, J.J. Cha, G. Zheng, Y. Yang, M.T. McDowell, P.C. Hsu, Y. Cui, Sulphur–TiO₂ yolk–shell nanoarchitecture with internal void space for long-cycle lithium–sulphur batteries, *Nat. Commun.* 4 (2013) 1331.
- [29] R. Ponraj, A.G. Kannan, J.H. Ahn, D.-W. Kim, Improvement of cycling performance of lithium–sulfur batteries by using magnesium oxide as a functional additive for trapping lithium polysulfide, *ACS Appl. Mater. Interfaces* 8 (2016) 4000–4006.
- [30] X. Liu, J.Q. Huang, Q. Zhang, L. Mai, Nanostructured metal oxides and sulfides for lithium–sulfur batteries, *Adv. Mater.* 29 (2017), 1601759.
- [31] W. Li, Z. Liang, Z. Lu, X. Tao, K. Liu, H. Yao, Y. Cui, Magnetic field-controlled lithium polysulfide semi-liquid battery with ferrofluidic properties, *Nano Lett.* 15 (2015) 7394.
- [32] Z. Gao, Y. Schwab, Y. Zhang, N. Song, X. Li, Ferromagnetic nanoparticle–assisted polysulfide trapping for enhanced lithium–sulfur batteries, *Adv. Funct. Mater.* 28 (2018) 1800563.
- [33] J. Zheng, J. Tian, D. Wu, M. Gu, W. Xu, C. Wang, F. Gao, M.H. Engelhard, J.G. Zhang, J. Liu, J. Xiao, Lewis acid–base interactions between polysulfides and metal organic framework in lithium sulfur batteries, *Nano Lett.* 14 (2014) 2345–2352.
- [34] Z. Wang, B. Wang, Y. Yang, Y. Cui, Z. Wang, B. Chen, G. Qian, Mixed-metal–organic framework with effective Lewis acidic sites for sulfur confinement in high-performance lithium–sulfur batteries, *ACS Appl. Mater. Interfaces* 7 (2015) 20999–21004.
- [35] Z.A. Ghazi, L. Zhu, H. Wang, A. Naeem, A.M. Khattak, B. Liang, N.A. Khan, Z. Wei, L. Li, Z. Tang, Efficient polysulfide chemisorption in covalent organic frameworks for high-performance lithium-sulfur batteries, *Adv. Energy Mater.* 6 (2016) 1601250.
- [36] J.W. Zhou, R. Li, X.X. Fan, Y.F. Chen, R.D. Han, W. Li, J. Zheng, B. Wang, X.G. Li, Rational design of a metal–organic framework host for sulfur storage in fast, long-cycle Li–S batteries, *Energy Environ. Sci.* 7 (2014) 2715–2724.
- [37] C. Li, Z. Li, Q. Li, Z. Zhang, S. Dong, L. Yin, MOFs derived hierarchically porous TiO₂ as effective chemical and physical immobilizer for sulfur species as cathodes for high-performance lithium–sulfur batteries, *Electrochim. Acta* 215 (2016) 689–698.
- [38] H. Park, D.J. Siegel, Tuning the adsorption of polysulfides in lithium–sulfur batteries with metal–organic frameworks, *Chem. Mater.* 29 (2017) 4932–4939.
- [39] S. Bai, X. Liu, K. Zhu, S. Wu, H. Zhou, Metal–organic framework-based separator for lithium–sulfur batteries, *Nat. Energy* 1 (2016) 16094.
- [40] S.H. Chung, P. Han, A. Manthiram, A polysulfide-trapping interface for electrochemically stable sulfur cathode development, *ACS Appl. Mater. Interfaces* 8 (2016) 4709–4717.
- [41] T. Yim, S.H. Han, N.H. Park, M.-S. Park, J.H. Lee, J. Shin, J.W. Choi, Y. Jung, Y.N. Jo, J.-S. Yu, K.J. Kim, Effective polysulfide rejection by dipole-aligned BaTiO₃ coated separator in lithium–sulfur batteries, *Adv. Funct. Mater.* 26 (2016) 7817–7823.
- [42] N.P. Deng, W.M. Kang, Y.B. Liu, J.G. Ju, D.Y. Wu, L. Li, B.S. Hassan, B.W. Cheng, A review on separators for lithium sulfur battery: progress and prospects, *J. Power Sources* 331 (2016) 132–155.
- [43] R. Ponraj, A.G. Kannan, J.H. Ahn, J.H. Lee, J. Kang, B. Han, D.-W. Kim, Effective trapping of lithium polysulfides using a functionalized carbon nanotube-coated separator for lithium–sulfur cells with enhanced cycling stability, *ACS Appl. Mater. Interfaces* 9 (2017) 38445–38454.
- [44] W.Z. Bao, Z.A. Zhang, Y.H. Qu, C.K. Zhou, X.W. Wang, J. Li, Confine sulfur in mesoporous metal–organic framework @ reduced graphene oxide for lithium sulfur battery, *J. Alloys Compd.* 582 (2014) 334–340.
- [45] Z.Q. Wang, Z.S. Dou, Y.J. Cui, Y. Yang, Z.Y. Wang, G.D. Qian, Sulfur encapsulated ZIF-8 as cathode material for lithium–sulfur battery with improved cyclability, *Microporous Mesoporous Mater.* 185 (2014) 92–96.
- [46] Z. Wang, B. Wang, Y. Yang, Y. Cui, Z. Wang, B. Chen, G. Qian, Mixed-metal–organic framework with effective Lewis acidic sites for sulfur confinement in high-performance lithium-sulfur batteries, *ACS Appl. Mater. Interfaces* 37 (2015) 20999–21004.
- [47] Q. Pang, X. Liang, C.Y. Kwok, L.F. Nazar, Advances in lithium–sulfur batteries based on multifunctional cathodes and electrolytes, *Nat. Energy* 1 (2016) 16132.
- [48] M. Diaz-Garcia, A. Mayoral, I. Diaz, M. Sanchez-Sanchez, Nanoscaled m-MOF-74 materials prepared at room temperature, *Cryst. Growth Des.* 14 (2014) 2479–2487.
- [49] S. Horike, D. Umeyama, S. Kitagawa, Ion conductivity and transport by porous coordination polymers and metal–organic frameworks, *Acc. Chem. Res.* 46 (2013) 2376–2384.
- [50] U. Kuila, M. Prasad, Specific surface area and pore-size distribution in clays and shales, *Geophys. Prospect.* 61 (2013) 341–362.
- [51] A. Bhaskar, M. Deepa, T.N. Rao, MoO₂/Multi-walled carbon nanotubes (MWCNT) hybrid for use as a Li-ion battery anode, *ACS Appl. Mater. Interfaces* 5 (2013) 2555–2566.
- [52] X. Lu, H. Dou, C. Yuan, S. Yang, L. Hao, F. Zhang, L. Shen, L. Zhang, X. Zhang, Polypyrrole/carbon nanotube nanocomposite enhanced the electrochemical capacitance of flexible graphene film for supercapacitors, *J. Power Sources* 197 (2012) 319–324.
- [53] Y.S. Su, A. Manthiram, A new approach to improve cycle performance of rechargeable lithium–sulfur batteries by inserting a free-standing MWCNT interlayer, *Chem. Commun.* 48 (2012) 8817–8819.
- [54] C.H. Chang, S.H. Chung, A. Manthiram, Ultra-lightweight PANiNF/MWCNT-functionalized separators with synergistic suppression of polysulfide migration for Li–S batteries with pure sulfur cathodes, *J. Mater. Chem. A* 3 (2015) 18829–18834.
- [55] H.M. Kim, J.Y. Hwang, A. Manthiram, Y.K. Sun, High-performance lithium–sulfur batteries with a self-assembled multiwalled carbon nanotube interlayer and a robust electrode–electrolyte interface, *ACS Appl. Mater. Interfaces* 8 (2016) 983–987.
- [56] X. Liang, C. Hart, Q. Pang, A. Garsuch, T. Weiss, L.F. Nazar, A highly efficient polysulfide mediator for lithium–sulfur batteries, *Nat. Commun.* 6 (2015) 5682.
- [57] A.P. Grosvenor, M.C. Biesinger, R.S. Smart, N.S. McIntyre, New interpretations of XPS spectra of nickel metal and oxides, *Surf. Sci.* 600 (2006) 1771–1779.
- [58] J. Jiang, J. Zhu, W. Ai, X. Wang, Y. Wang, C. Zou, W. Huang, T. Yu, Encapsulation of sulfur with thin-layered nickel-based hydroxides for long-cyclic lithium–sulfur cells, *Nat. Commun.* 6 (2015) 8622.